Available online at www.sciencedirect.com
SCIENCE DIRECT®
Journal of Solid State Chemistry 177 (2004) 4359–4367
JOURNAL OF SOLID STATE CHEMISTRY
www.elsevier.com/locate/jssc

Defect and dopant properties of $MgTa_2O_6$

Cristina Tealdi[a], M. Saiful Islam[b], Lorenzo Malavasi[a,*], Giorgio Flor[a]

[a]*Dipartimento di Chimica Fisica "M. Rolla", Università degli Studi di Pavia, Viale Taramelli, No. 16, PV 27100, Pavia, Italy*
[b]*Department of Chemistry, University of Surrey, Guildford, GU2 7XH, United Kingdom*

Received 17 May 2004; received in revised form 29 June 2004; accepted 29 June 2004

Abstract

Atomistic computer simulation techniques have been used, for the first time, to reproduce the crystal structure of $MgTa_2O_6$ and to investigate the defect chemistry and dopant properties of this material. The calculated defect energetics suggest that the concentration of intrinsic atomic defects in this phase is insignificant and that the system is probably stable to both oxidation and reduction. Dopant solution energy versus ion size trends are found for both isovalent and aliovalent dopant incorporation at Mg and Ta sites. Divalent dopants (e.g. Ca, Cu) preferentially occupy the Mg site whereas dopants with higher charge (e.g. Sc, Zr, Nb) are more favorable on the Ta site. High migration activation energies (>2 eV) predict limited ionic conductivity in this material.

Keywords: Magnesium Tantalate; Atomistic Simulation; Defect Chemistry

1. Introduction

Dielectric oxides have been of significant interest during the last 50 years and the research field is still in expansion, due to their wide range of technological applications. In particular, materials with high dielectric constant and low dielectric loss at microwave frequency can be used as a dielectric resonator, as was first proposed by Richtmyer [1]. Complex perovskite-related structures, based on Nb and Ta, are extensively known for their microwave dielectric properties [2–6]. More recent studies [7–9] have focused attention on oxides of general formula AB_2O_6 and crystallizing in the columbite or trirutile structure, suggesting their use as microwave dielectric resonators in satellite communication [10,11]. Besides their direct applications, these phases are important intermediates during the synthesis of perovskite-related structures by the synthesis route known as the *columbite precursor method* [12–14]. Furthermore, alkaline earth tantalates, in particular $MgTa_2O_6$ and $BaTa_2O_6$, have attracted interest because of their photocatalytic activities for water decomposition without co-catalysts [15].

Despite the numerous studies on AB_2O_6 phases and their applications, there has been limited work related to the defect structure and transport properties of these materials at the atomic level. Moreover, computational studies of these phases have not been carried out previously and this work presents the first atomistic modelling study of AB_2O_6-type tantalates. These simulation techniques are well established and have been successfully applied to numerous other structures, such as ceria-based catalysts [16,17], $LaMO_3$ perovskite oxides [18–21] and Bi Aurivillius phases (e.g., $Bi_4Ti_3O_{12}$) [22]. In the present study, we focused our attention on the $MgTa_2O_6$ phase, which crystallizes in a tetragonal structure. We have attempted to clarify the defect structure of this complex ternary oxide by examining the energetics of intrinsic defects, redox reactions, dopant ion substitution and ion migration.

*Corresponding author. Fax: +39-0382-507-575.
E-mail address: lorenzo.malavasi@unipv.it (L. Malavasi).

0022-4596/$ - see front matter © 2004 Elsevier Inc. All rights reserved.
doi:10.1016/j.jssc.2004.06.055

2. Simulation methods

The simulation techniques used in this work are based upon lattice energy minimization procedures, embodied in the GULP code [23]. Only a brief summary of the important aspects of these techniques will be presented as comprehensive reviews are given elsewhere [24,25].

The basis of the simulation is the specification of a potential model which describes the energy of the system as a function of the atomic coordinates and allows the modelling of perfect and defective lattices. The interactions between ions are partitioned in terms of long range Coulombic forces and short range interactions which account for electron cloud overlap (Pauli repulsion) and dispersion (Van der Waals) interactions. An analytical function of the Buckingham form (Eq. (1)) contains the short-range potential parameters which are usually empirically derived values:

$$V = A_{ij} \exp(-r/\rho_{ij}) - C_{ij}/r^6. \quad (1)$$

Ionic polarization is treated using the "shell" model developed by Dick and Overhauser [26]. This model includes coupling between the short-range repulsive forces and ionic polarization and has been shown to simulate effectively both dielectric and elastic properties.

The calculation of defect formation and migration energies utilizes the Mott–Littleton approach, in which the crystal lattice is partitioned into two regions: a spherical inner region with the defect in its center (region I) and an outer region extended to infinity (region II). Whereas in region I the interactions are calculated explicitly, the response of region II to the defect can be treated by more approximate quasi-continuum methods. For the calculations presented here, region I was defined as to contain about 380 ions, which is expected to give reliable convergence of defect formation and migration energies.

3. Results and discussion

3.1. Structural modelling

The ternary oxide $MgTa_2O_6$ crystallises in the space group $P4_2/mnm$ [27]. The crystal structure (Fig. 1) is described by a unit cell which is triple that of the conventional rutile unit cell along the tetragonal c-axis. The cations, which occupy half of the octahedral available sites, are surrounded by O^{2-} organized in a hexagonal close-packed arrangement. This results in a chemically ordered network of interpenetrating edge and corner-sharing slightly distorted octahedra. Successive Mg–O planes (at $z = 0$ and 0.5) are separated by two Ta–O planes ($z \sim 1/6$ and $z \sim 1/3$).

Using the simulation approach described above, the crystal structure of $MgTa_2O_6$ has been modelled. The starting Buckingham potential and the shell-model parameters [28–30] have been slightly refined in order to reproduce the structure. The resulting potentials, listed in Table 1, succeeded in carefully reproducing the atomic positions within the structure. In Table 2 the comparison between the experimental [27] and calculated structures is presented. The agreement between the experimental bond lengths and the calculated values shows that the model used can reproduce the complex structure of $MgTa_2O_6$, particularly the octahedral distortion around the cations. This potential model

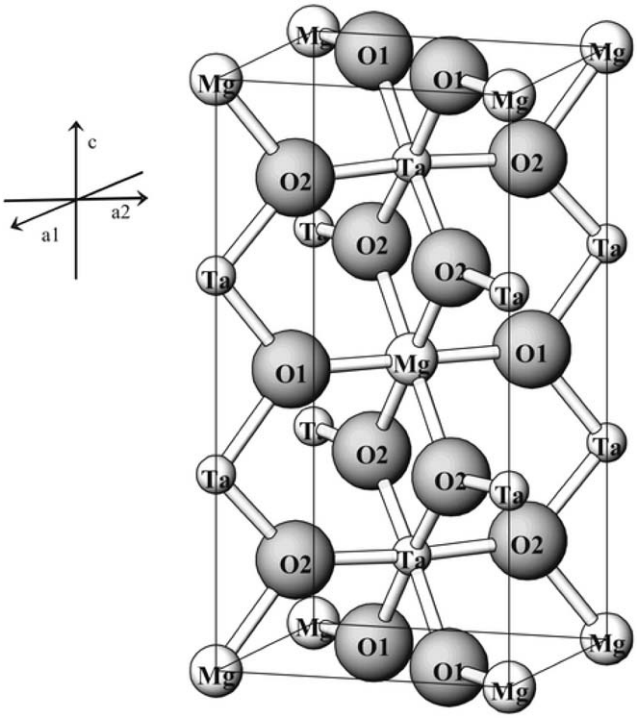

Fig. 1. Unit cell of the tetragonal $MgTa_2O_6$ structure.

Table 1
Interatomic (Buckingham) potentials and shell-model parameters for $MgTa_2O_6$

Interaction	A (eV)	ρ (Å)	C (eV Å^6)	Y (e)	K (eV Å^{-2})	Reference
$Mg^{2+}\cdots O^{2-}$	821.60	0.2950	0.00	2.00	99999.00	This study
$Ta^{5+}\cdots O^{2-}$	1315.57	0.3690	0.00	−4.59	5916.57	[29]
$O^{2-}\cdots O^{2-}$	9547.96	0.2191	32.00	−2.04	42.00	[30]

Table 2
Comparison between experimental and calculated structures of $MgTa_2O_6$

Parameter	Experimental [28]	Calculated	Δ (exp-calc)
a (Å)	4.719	4.570	0.149
b (Å)	4.719	4.570	0.149
c (Å)	9.200	9.704	−0.504
V (Å^3)	204.900	202.700	2.200
Ta z	0.3319	0.333	−0.001
O1 x	0.308	0.314	−0.006
O1 y	0.308	0.314	−0.006
O2 x	0.297	0.301	−0.004
O2 y	0.297	0.301	−0.004
O2 z	0.323	0.321	0.002
Mg–O1 (x2) (Å)	2.055	2.032	0.023
Mg–O2 (x4) (Å)	2.118	2.163	−0.045
Ta–O1 (x2) (Å)	2.008	2.018	−0.010
Ta–O2 (x2) (Å)	1.966	1.950	0.016
Ta–O2 (x2) (Å)	1.984	1.967	0.017

therefore provides a valid starting point for our subsequent defect calculations.

3.2. Intrinsic atomic defects

The energies of isolated point defects in the $MgTa_2O_6$ structure were first calculated. Since there are no previous studies of the defect structure of this and related materials, different interstitial sites were also considered. Results show that the most favorable interstitial site for both Mg and Ta is at an octahedral-type position at (0, 1/2, 0) whereas the O interstitial site is placed at a tetrahedral-type position (0, 1/2, 1/4), as shown in Fig. 2. The defect energy for both vacancies and interstitials are listed in Table 3.

There are two non-equivalent oxygen sites (labelled O1 and O2) in the structure and hence two different oxygen vacancy energies; the difference in energy between these two values is about 2 eV, reflecting an appreciable distortion in the structure. The most favorable energy is associated with oxygen vacancies on the O1 site.

Frenkel and Schottky-type energies were then derived by combining the individual defect energies and the appropriate lattice energies. The defect reactions are given below (Eqs. (2)–(7)) and the corresponding energies are listed in Table 4.

Magnesium Frenkel disorder:

$$Mg_{Mg}^{x} \rightarrow V_{Mg}'' + Mg_i^{\cdot\cdot}. \quad (2)$$

Tantalum Frenkel disorder:

$$Ta_{Ta}^{x} \rightarrow V_{Ta}^{5'} + Ta_i^{5\cdot} \quad (3)$$

Oxygen Frenkel disorder:

$$O_O^{x} \rightarrow V_O^{\cdot\cdot} + O_i''. \quad (4)$$

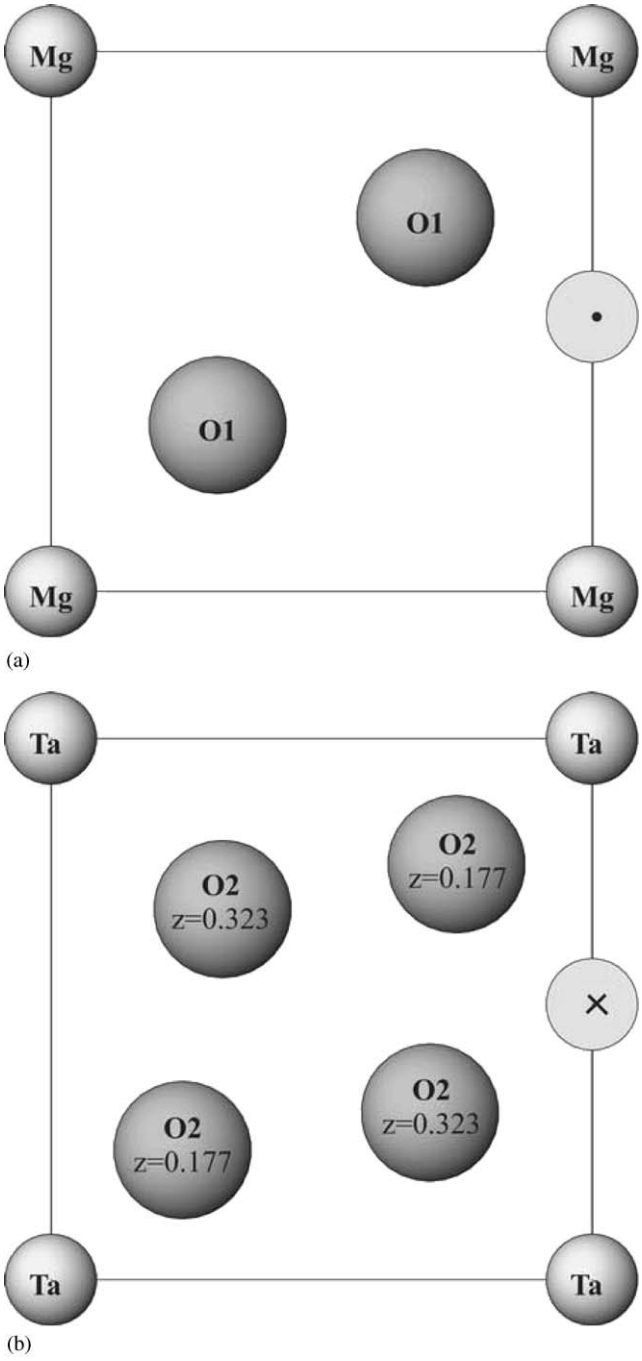

Fig. 2. Possible interstitial positions in the $MgTa_2O_6$ structure: (a) octahedral site (dot) and (b) tetrahedral site (cross). Projection of the structure along the c-axis.

$MgTa_2O_6$ full Schottky disorder:

$$Mg_{Mg}^{x} + 2Ta_{Ta}^{x} + 6O_O^{x} \rightarrow V_{Mg}'' + 2V_{Ta}^{5'} + 6V_O^{\cdot\cdot} + MgTa_2O_6^{surf}. \quad (5)$$

MgO partial Schottky-type disorder:

$$Mg_{Mg}^{x} + O_O^{x} \rightarrow V_{Mg}'' + V_O^{\cdot\cdot} + MgO^{surf}. \quad (6)$$

Table 3
Calculated isolated defect energies for $MgTa_2O_6$

Site	Vacancy (eV)	Interstitial (eV)
Mg	32.63	−27.90
Ta	130.97	−107.77
O1	17.62	−10.47
O2	19.99	−10.47

Table 4
Energies of Frenkel and Schottky disorder in $MgTa_2O_6$

Reaction	Equation	E (eV/defect)
Mg Frenkel	2	2.37
Ta Frenkel	3	11.60
O Frenkel	4	3.58
$MgTa_2O_6$ full Schottky	5	4.45
MgO partial Schottky	6	4.48
Ta_2O_5 partial Schottky	7	4.65

Ta_2O_5 partial Schottky-type disorder:

$$2Ta_{Ta}^{x} + 5O_{O}^{x} \rightarrow 2V_{Ta}^{5'} + 5V_{O}^{\cdot\cdot} + Ta_2O_5^{surf}. \quad (7)$$

Examination of the results (Table 4) suggests that Mg Frenkel disorder is the most favorable intrinsic defect with the lowest formation energy, although the magnitude is still relatively high. In contrast, Ta Frenkel disorder is the most unlikely, probably due to the extremely high charge of this cation. Schottky disorder involving either anion or cation vacancies are also found to be unfavorable. In general, the high magnitude of our calculated energies suggests that the concentration of intrinsic atomic defects in $MgTa_2O_6$ will not be significant.

3.3. Redox reactions

In addition to intrinsic Schottky and Frenkel disorder, possible oxidation and reduction mechanisms in the $MgTa_2O_6$ system were analyzed. For the undoped system the following reaction equations were considered (normalised to $1/2O_2$):

$$\tfrac{1}{2}O_{2(g)} \rightarrow O_i'' + 2h^{\cdot}, \quad (8)$$

$$\tfrac{1}{2}O_{2(g)} + Mg_{Mg}^{x} \rightarrow V_{Mg}'' + 2h^{\cdot} + MgO \quad (9)$$

$$\tfrac{1}{2}O_{2(g)} + \tfrac{2}{5}Ta_{Ta}^{x} \rightarrow \tfrac{2}{5}V_{Ta}^{5'} + 2h^{\cdot} + \tfrac{1}{5}Ta_2O_5, \quad (10)$$

$$O_{O}^{x} \rightarrow V_{O}^{\cdot\cdot} + \tfrac{1}{2}O_{2(g)} + 2e'. \quad (11)$$

The approach to electronic defects in the magnesium tantalate is similar to previous work [17,21] and is based on localized species with the hole centers ($h^{\cdot}$) modelled as O^{-} and the electron centers (e') as Ta^{4+}. For this approach, the appropriate ionization energies for O and Ta must be used. Unfortunately, no values of the fifth ionization energy for Ta have been reported in the literature. We have extrapolated this value from the relative trend of V and Nb ionization energies and the known values of the first three ionization energies for Ta. Although we must be cautious in considering detailed interpretations of the reduction process, our approach provides useful trends in defect-redox properties.

Table 5
Calculated energies for redox processes in $MgTa_2O_6$

Redox process	E (eV/electron)[a]
Oxidation 8	8.45
Oxidation 9	8.25
Oxidation 10	7.02
Reduction 11	13.82

[a]Hole term (7.65 eV); electron term (9.94 eV); $\frac{1}{2}O_2 \rightarrow O$ (9.86 eV).

Using the appropriate electronic and energetic terms, the energies of the redox reactions were calculated (listed in Table 5). These results predict that, due to the extremely high-energy values, the system is stable to both oxidation and reduction. This suggests that the formation of intrinsic electronic defects is unlikely and hence electronic conductivity in this system will not be significant. Our results on intrinsic atomic and electronic defects suggest that the defect chemistry of $MgTa_2O_6$ would be dominated by the addition of dopants, which we consider in the next section.

3.4. Dopant substitution

A wide range of isovalent and aliovalent substitutions on both Mg and Ta sites have been studied. The dopant incorporation mechanism, which in the case of aliovalent substitution requires the creation of oxygen vacancies or interstitials for charge-compensation, follows the reaction equations reported below (Eqs. (12)–(19)):

(i) M^{2+} dopants at Mg and Ta

$$MO + Mg_{Mg}^{x} \rightarrow M_{Mg}^{x} + MgO, \quad (12a)$$

$$E_{solution} = E(M_{Mg}^{x}) + U_{lattice}(MgO) - U_{lattice}(MO), \quad (12b)$$

$$2MO + 2Ta_{Ta}^{x} + 3O_{O}^{x} \rightarrow 2M_{Ta}^{'''} + 3V_{O}^{\cdot\cdot} + Ta_2O_5, \quad (13a)$$

$$E_{solution} = E(M_{Ta}^{'''}) + \tfrac{3}{2}E(V_{O}^{\cdot\cdot}) + \tfrac{1}{2}U_{lattice}(Ta_2O_5) - U_{lattice}(MO). \quad (13b)$$

(ii) M^{3+} dopants at Mg and Ta

$$M_2O_3 + 2Mg^x_{Mg} \rightarrow 2M^{\cdot}_{Mg} + O''_i + 2MgO, \quad (14a)$$

$$E_{solution} = E(M^{\cdot}_{Mg}) + \tfrac{1}{2}E(O''_i) + U_{lattice}(MgO) - \tfrac{1}{2}U_{lattice}(M_2O_3), \quad (14b)$$

$$M_2O_3 + 2Ta^x_{Ta} + 2O^x_O \rightarrow 2M''_{Ta} + 2V^{\cdot\cdot}_O + Ta_2O_5, \quad (15a)$$

$$E_{solution} = E(M''_{Ta}) + E(V^{\cdot\cdot}_O) + \tfrac{1}{2}U_{lattice}(Ta_2O_5) - \tfrac{1}{2}U_{lattice}(M_2O_3). \quad (15b)$$

(iii) M^{4+} dopants at Mg and Ta

$$MO_2 + Mg^x_{Mg} \rightarrow M^{\cdot\cdot}_{Mg} + O''_i + MgO, \quad (16a)$$

$$E_{solution} = E(M^{\cdot\cdot}_{Mg}) + E(O''_i) + U_{lattice}(MgO) - U_{lattice}(MO_2), \quad (16b)$$

$$2MO_2 + 2Ta^x_{Ta} + O^x_O \rightarrow 2M'_{Ta} + V^{\cdot\cdot}_O + Ta_2O_5, \quad (17a)$$

$$E_{solution} = E(M'_{Ta}) + \tfrac{1}{2}E(V^{\cdot\cdot}_O) + \tfrac{1}{2}U_{lattice}(Ta_2O_5) - U_{lattice}(MO_2). \quad (17b)$$

(iv) M^{5+} dopants at Mg and Ta

$$M_2O_5 + Mg^x_{Mg} \rightarrow 2M^{\cdot\cdot\cdot}_{Mg} + 3O''_i + 2MgO, \quad (18a)$$

$$E_{solution} = E(M^{\cdot\cdot\cdot}_{Mg}) + \tfrac{3}{2}E(O''_i) + U_{lattice}(MgO) - \tfrac{1}{2}U_{lattice}(M_2O_5), \quad (18b)$$

$$M_2O_5 + 2Ta^x_{Ta} \rightarrow 2M^x_{Ta} + Ta_2O_5, \quad (19a)$$

$$E_{solution} = E(M^x_{Ta}) + \tfrac{1}{2}U_{lattice}(Ta_2O_5) - \tfrac{1}{2}U_{lattice}(M_2O_5). \quad (19b)$$

Alternative compensation mechanisms via cation vacancy formation have been considered for aliovalent substitution on the Mg site, but the results show that they are not favorable.

The dopant reaction or "solution" energies can be calculated by combining appropriate defect and lattice energy terms. The interatomic Buckingham potentials (Table 6) and the lattice energies (Table 7) used for all the dopant species are derived from previous related studies [18–21,28–32]. In Fig. 3 the solution energies as a function of the dopant ionic radius are reported for the wide range of substitutions considered. We are aware that, due to the uncertainty in the precise magnitude of the lattice energies that have been used, the relative trends are more significant than the absolute values reported. The plots shown in Fig. 3 reveal two main points.

Table 6
Buckingham potentials and shell-model parameters for dopant ions

Interaction	A (eV)	ρ (Å)	C (eV Å^6)	Y (e)	K (eV Å^{-2})
$Ca^{2+}\cdots O^{2-}$	1090.4	0.3372	0.00	1.26	34.00
$Sr^{2+}\cdots O^{2-}$	1400.0	0.3500	0.00	1.33	21.53
$Ba^{2+}\cdots O^{2-}$	931.79	0.3949	0.00	1.46	14.78
$Mn^{2+}\cdots O^{2}$	715.8	0.3464	0.00	3.00	81.20
$Fe^{2+}\cdots O^{2-}$	694.1	0.3399	0.00	2.00	10.92
$Co^{2+}\cdots O^{2}$	696.3	0.3362	0.00	2.00	10.74
$Ni^{2+}\cdots O^{2}$	683.5	0.3332	0.00	2.00	8.77
$Cu^{2+}\cdots O^{2}$	3799.3	0.2427	0.00	2.00	99999.00
$Zn^{2+}\cdots O^{2}$	499.6	0.3595	0.00	2.05	10.28
$Al^{3+}\cdots O^{2-}$	1114.9	0.3118	0.00	3.00	99999.00
$Fe^{3+}\cdots O^{2-}$	1156.36	0.3299	0.00	4.97	304.70
$Co^{3+}\cdots O^{2-}$	1329.82	0.3087	0.00	3.00	196.30
$Mn^{3+}\cdots O^{2-}$	1267.50	0.3214	0.00	4.97	304.70
$Sc^{3+}\cdots O^{2-}$	1299.4	0.3312	0.00	3.00	99999.00
$Yb^{3+}\cdots O^{2-}$	1309.6	0.3462	0.00	3.00	99999.00
$Ti^{4+}\cdots O^{2-}$	877.2	0.38096	9.0	−35.86	95.00
$Sn^{4+}\cdots O^{2-}$	1056.8	0.3683	0.00	1.58	2037.80
$Zr^{4+}\cdots O^{2-}$	985.869	0.3760	0.00	1.35	169.617
$Ce^{4+}\cdots O^{2-}$	1986.83	0.3511	20.40	7.70	29175.00
$Nb^{5+}\cdots O^{2-}$	1796.3	0.34598	0.00	−4.49	1358.58

Table 7
Solution energies for dopant substitution in $MgTa_2O_6$

Dopant	Lattice energy (eV)	Solution energy (eV/dopant)	
		Mg site	Ta site
Mg^{2+}	−41.29	—	8.13
Ca^{2+}	−35.95	2.47	12.31
Sr^{2+}	−33.42	3.50	13.95
Ba^{2+}	−33.74	8.34	23.11
Ni^{2+}	−41.58	3.43	14.17
Cu^{2+}	−43.79	2.39	11.87
Zn^{2+}	−39.80	2.78	12.87
Co^{2+}	−40.83	3.15	13.65
Fe^{2+}	−40.12	2.87	13.13
Mn^{2+}	−38.73	2.50	12.45
Al^{3+}	−160.50	12.77	8.23
Fe^{3+}	−150.85	12.60	7.82
Mn^{3+}	−150.82	10.65	6.45
Sc^{3+}	−144.47	9.86	5.80
Yb^{3+}	−136.76	10.25	6.19
Ti^{4+}	−112.45	10.12	4.49
Sn^{4+}	−110.68	9.14	2.51
Zr^{4+}	−109.76	9.43	3.03
Ce^{4+}	−105.66	11.13	6.19
Nb^{5+}	−322.00	28.35	0.63
Ta^{5+}	−317.51	27.82	—

Lattice energies values refer to the parent oxides.

First, divalent dopants (such as Cu, Ni, Zn, Ca) are more favorable at the isovalent Mg site than at the Ta site. We note that incorporation of the large Ba^{2+} is unlikely at either site.

Second, the M^{3+}, M^{4+} and M^{5+} dopants considered would preferentially occupy the Ta site (with oxygen vacancy compensation for aliovalent substitution). However, the higher energies for M^{3+} ions suggest relatively lower solubility at the Ta site. We predict that possible dopants that are worth investigating further include Sc^{3+}, Zr^{4+}, Sn^{4+} and Nb^{5+}.

For completeness we also considered anti-site disorder, which corresponds to the inversion of the site position between Mg^{2+} and the Ta^{5+} according to the following equation:

$$Mg_{Mg}^{x} + Ta_{Ta}^{x} \rightarrow Ta_{Mg}^{'''} + Mg_{Ta}^{\cdots}. \quad (20)$$

The calculations suggest that this is a highly unfavorable process ($E_{inv} \sim 8$ eV). This result may help to rationalise the experimental difficulty in synthesizing samples of these phases with partial anti-site disorder.

3.5. Ion migration

Doping on the Ta site with tetravalent cations seems to be the most favorable mechanism to increase the oxygen vacancy concentration. A higher concentration of vacancies may make the ionic transport appreciable in this structure. We therefore examined the energetics of vacancy migration in $MgTa_2O_6$.

The energy profiles are mapped out by calculating the defect energy of the migrating ion at different points along the migration path; an example profile is shown in Fig. 4. The migration of each ion has been assumed to follow a linear path between two nearest neighbor sites and, indeed, no significant deviations from this pathway have been detected. In Table 8 the activation energies for each migration path are listed. All the vacancy paths show high migration energies (>2 eV), predicting that the system is unlikely to exhibit appreciable ionic conductivity. Results show that the lowest activation energy for vacancy migration is associated with Mg, although the concentration of Mg vacancies in this system is unlikely to be sufficient to induce considerable ionic transport.

We also considered interstitial migration of each species in order to achieve a complete description of the ionic transport in this structure. The corresponding activation energies are summarized in Table 6 with another example energy profile shown in Fig. 4. It is clear, however, that interstitial migration of all the ion species is predicted to be very unlikely, with high activation energies (>3.9 eV). In general, the results suggest that ionic conduction will not be significant in $MgTa_2O_6$.

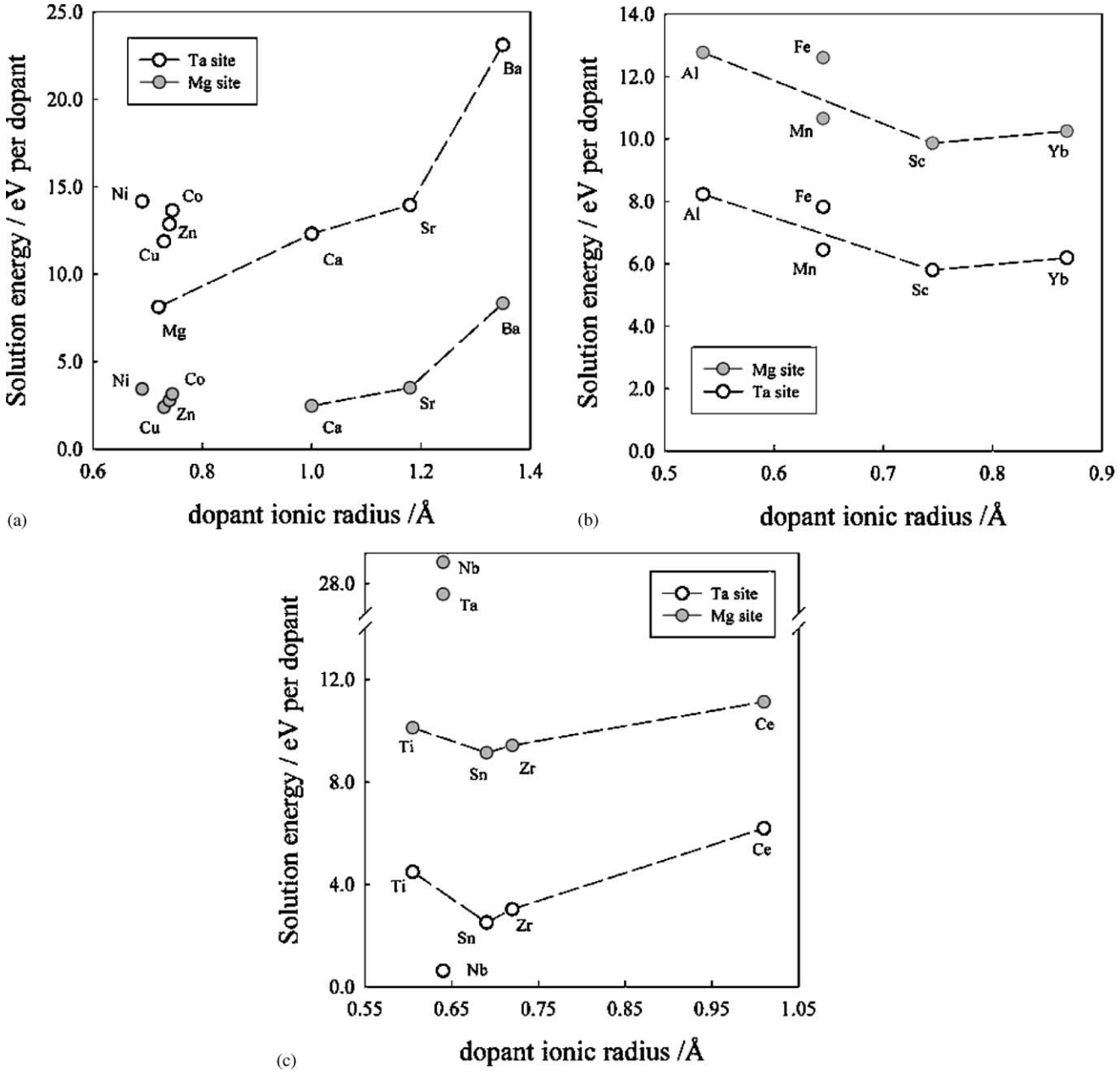

Fig. 3. Solution energies versus ionic radius for a range of cation dopants at both Mg and Ta sites: (a) M^{2+} dopant, (b) M^{3+} dopant and (c) M^{4+} and M^{5+} dopants. (Lines are guides to the eye.)

4. Conclusion

The present study demonstrates how atomistic simulation techniques can contribute to the understanding of the defect chemistry and the dopant properties of $MgTa_2O_6$. Since this is the first attempt to model this structure, our discussion has drawn attention to the following basic concepts that are of relevance to potential dielectric or catalytic applications:

1. The lattice simulations reproduce the observed complex structure of $MgTa_2O_6$ and the local distortion of the octahedral coordination around the cations. We predict that the lowest energy disorder is the Mg Frenkel defect, although the relative magnitude is still high, suggesting that the concentration of intrinsic atomic defects will not be significant. The energies of redox reactions suggest that the system is probably stable to both oxidation and reduction.
2. A range of isovalent and aliovalent substitutions on Mg and Ta sites have been considered. The results reveal that divalent dopants (e.g. Ni, Cu, Ca) are more favorable at the isovalent Mg site than the Ta

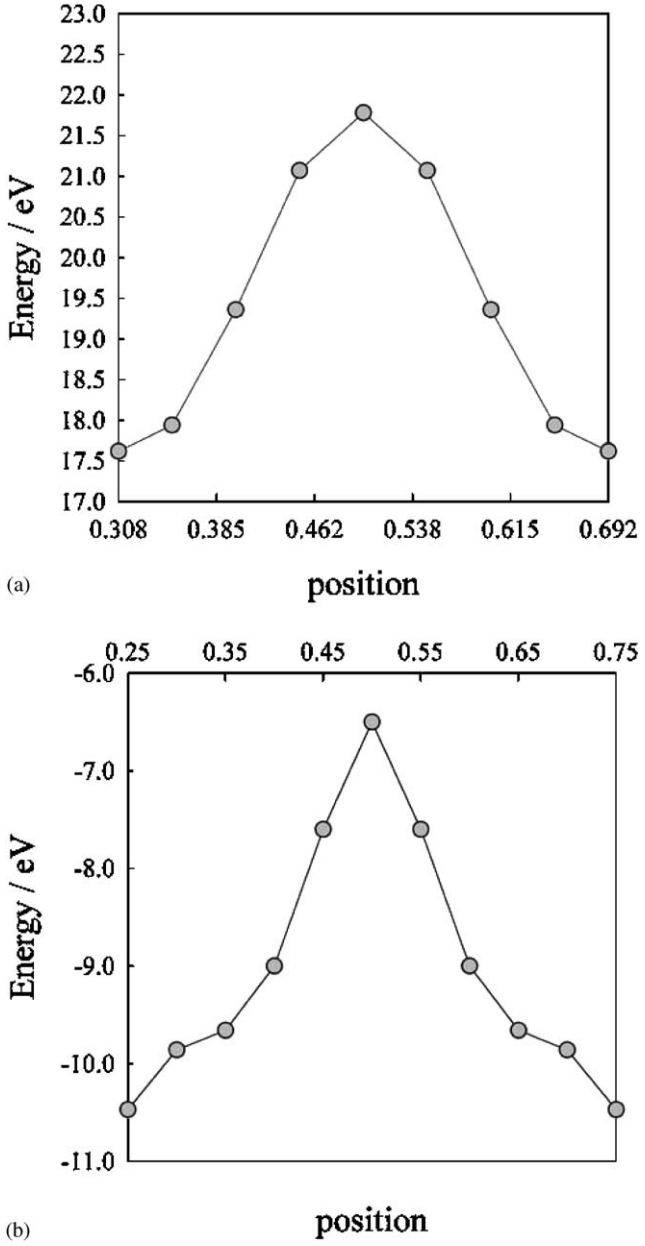

Fig. 4. Energy profiles for ion migration paths: (a) O–O vacancy and (b) O^{2-} interstitial.

site, with the incorporation of the large Ba^{2+} unlikely at either site. The M^{3+}, M^{4+} and M^{5+} dopants are predicted to preferentially occupy the Ta site. Aliovalent substitution on the Ta site (e.g., Zr, Sn) is compensated by oxygen vacancies. Possible dopants that are worth further experimental investigation include Sc^{3+}, Zr^{4+}, Sn^{4+} and Nb^{5+}.

3. Calculated migration activation energies for all three species (Mg, Ta, O) are greater than 2 eV for vacancy and interstitial mechanisms. This suggests that ionic conduction will not be significant in this material. This result, together with the predicted relative stability towards both oxidation and reduction, is in agreement with the peculiar low dielectric loss found in the magnesium tantalate.

Table 8
Calculated activation energies for vacancy and interstitial migration in $MgTa_2O_6$

	Mechanism	Activation energy (eV)
Vacancy	Mg	2.21
	Ta	3.04
	O1	4.16
	O2	2.47
Interstitial	Mg	4.50
	Ta	3.97
	O	9.14

In conclusion, this study provides a valuable starting point for the defect modelling of related phases, although attempts to simulate highly distorted AB_2O_6 compounds containing niobium instead of tantalum have proved difficult. Nevertheless, $MgTa_2O_6$ is one of the most important members of this class of compounds, and a key aim of this study is to encourage further experimental work in this area.

Acknowledgments

This work was financially supported by the Italian Ministry of Scientific Research (MIUR) by FIRB Projects (2001). The simulations were carried out on the computing facilities at Rutherford Appleton Laboratory. We are grateful to Dr. Julian Tolchard for useful discussions.

References

[1] R.D. Richtmyer, J. Appl. Phys. 10 (1939) 391–398.
[2] S. Nomura, K. Toyama, K. Kaneta, Jpn. J. Appl. Phys. 21 (1982) L624–L626.
[3] M. Onoda, J. Kuwata, K. Kaneta, K. Toyama, S. Nomura, Jpn. J. Appl. Phys. 21 (1982) 1707–1710.
[4] E.S. Kim, K.H. Yoon, Ferroelectrics 133 (1992) 187–192.
[5] T.V. Kolodiazhnyi, A. Petric, A.G. Belous, O. V'yunov, O. Yanchevskij, J. Mater. Res. 17 (2002) 3182–3189.
[6] D.C. Sun, S. Senz, D. Hesse, J. Eur. Ceram. Soc. 24 (2004) 2453–2463.
[7] A. Kan, H. Ogawa, H. Ohsato, J. Alloy. Compds. 337 (2002) 303–308.
[8] M. Thirumal, A.K. Ganguli, Prog. Cryst. Growth Charact. Mater. 44 (2002) 147–154.
[9] M. Thirumal, A.K. Ganguli, Mater. Res. Bull. 36 (2001) 2421–2427.
[10] H.J. Lee, I.T. Kim, K.S. Hong, Jpn. J. Appl. Phys.2 36 (10A) (1997) L1318–L1320.

[11] H.J. Lee, K.S. Hong, S.J. Kim, I.T. Kim, Mater. Res. Bull. 32 (1997) 847–855.
[12] F. Gu, Y. Shen, X.F. Liang, Mater. Sci. Eng. B-Solid State Mater. Adv. Technol. 99 (2003) 453–456.
[13] T.V. Kolodiazhnyi, A. Petric, G.P. Johari, A.G. Belous, J. Eur. Ceram. Soc. 22 (2002) 2013–2021.
[14] M.H. Liang, C.T. Hu, C.G. Chiou, Y.N. Tsai, I.N. Lin, Jpn. J. Appl. Phys. 1 38 (1999) 5621–5624.
[15] H. Kato, A. Kudo, Chem. Phys. Lett. 295 (1998) 487–492.
[16] M.S. Islam, G. Balducci, in: A. Trovarelli (Ed.), Catalysis by Ceria and Related Materials, Imperial College Press, London, 2002.
[17] G. Balducci, M.S. Islam, J. Kaspar, P. Fornasiero, M. Graziani, Chem. Mater. 15 (2003) 3781–3785.
[18] M.S.D. Read, M.S. Islam, G. Watson, F. King, F.E. Hancock, J. Mater. Chem. 10 (2000) 2298–2305.
[19] R.A. De Souza, M.S. Islam, E. Ivers-Tiffee, J. Mater. Chem. 9 (1999) 1621–1627.
[20] M.S. Islam, J. Mater. Chem. 10 (2000) 1027–1038.
[21] M.S. Islam, R.A. Davies, J. Mater. Chem. 14 (2004) 86–93.
[22] A. Sneddon, P. Lightfoot, T. Dinges, M.S. Islam, J. Solid State Chem. (2004), in press.
[23] J.D. Gale, J. Chem. Soc., Faraday Trans. 93 (1997) 629–637.
[24] C.R.A. Catlow, W.C. Mackrodt (Eds.), Computer Simulation of Solid, Lecture Notes in Physics, Springer, Berlin, 1982.
[25] C.R.A. Catlow, in: A.K. Cheetham, P. Day (Eds.), Solid State Chemistry-Techniques, Clarendon Press, Oxford, 1987, p. 231.
[26] B.G. Dick, A.W. Overhouser, Phys. Rev. 112 (1958) 90–103.
[27] G. Halle, H. Mullerbuschbaum, J. Less-Common. Met. 142 (1988) 263–268.
[28] G.V. Lewis, C.R.A. Catlow, J. Phys. C: Solid State Phys. 18 (1985) 1149–1161.
[29] H. Donnenberg, M. Exner, C.R.A. Catlow, Phys. Rev. B. 47 (1993) 14–19.
[30] C. Pirovano, M.S. Islam, R.N. Vannier, G. Nowogrocki, G. Mairesse, Solid State Ion 140 (2001) 115–123.
[31] C.M. Freeman, C.R.A. Catlow, J. Solid State Chem. 85 (1990) 65–75.
[32] R.C. Baetzold, Phys. Rev. B. 48 (1993) 5789–5796.